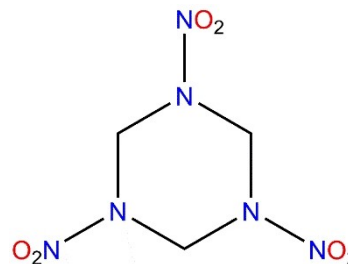


# The Elusive Ketene (H<sub>2</sub>CCO) Channel in the Infrared Multiphoton Dissociation of Solid 1,3,5-Trinitro-1,3,5-Triazinane (RDX)

Santosh K. Singh,<sup>[a]</sup> Jesse La Jeunesse,<sup>[a]</sup> Vasant Vuppuluri,<sup>[b]</sup> Steven F. Son,<sup>[b]</sup> Bing-Jian Sun,<sup>[c]</sup> Yue-Lin Chen,<sup>[c]</sup> Agnes H. H. Chang,<sup>[c]</sup> Alexander M. Mebel,<sup>[d]</sup> and Ralf I. Kaiser\*<sup>[a]</sup>

Understanding of the fundamental mechanisms involved in the decomposition of 1,3,5-trinitro-1,3,5-triazinane (RDX) still represents a major challenge for the energetic materials and physical (organic) chemistry communities mainly because multiple competing dissociation channels are likely involved and previous detection methods of the products are not isomer selective. In this study we exploited a microsecond pulsed infrared laser to decompose thin RDX films at 5 K under mild conditions to limit the fragmentation channels. The subliming decomposition products during the temperature programed desorption phase are detected using isomer selective single photoionization time-of-flight mass spectrometry (PI-ReTOF-MS). This technique enables us to assign a product signal at  $m/z=42$  to ketene (H<sub>2</sub>CCO), but not to diazomethane (H<sub>2</sub>CNN; 42 amu) as speculated previously. Electronic structure calculations support our experimental observations and unravel the decomposition mechanisms of RDX leading eventually to the elusive ketene (H<sub>2</sub>CCO) via an exotic, four-membered ring intermediate. This study highlights the necessity to exploit isomer-selective detection schemes to probe the true decomposition products of nitramine-based energetic materials.

For the last decades, the elucidation of the fundamental decomposition mechanisms of cyclic nitramines such as 1,3,5-trinitro-1,3,5-triazinane (RDX, Scheme 1) have received considerable attention from the material sciences, physical (organic), and theoretical chemistry communities due to their high energy content and vital applications as explosives and rocket



Scheme 1. Molecular structure of 1,3,5-trinitro-1,3,5-triazinane (RDX).

propellants.<sup>[1]</sup> An investigation of the central pathways involved in the fragmentation of RDX in the condensed phase and an identification of the primary and higher order reaction products, among them carbon-, nitrogen-, and oxygen-centered free radicals, which are formed in these processes, still represents a major challenge. These data are very much required by the physical (organic) and energetic material communities to unravel elementary mechanisms and bond breaking processes, which trigger the decomposition of energetic molecules. Multiple experimental and theoretical studies have been performed to elucidate the complex decomposition mechanism(s) of RDX.<sup>[2]</sup> Ultraviolet (UV) photodissociation of RDX was explored in the gas phase and in the condensed phase at discrete wavelengths of 226, 248, 236, and 229 nm. The majority of these studies revealed that the N–NO<sub>2</sub> bond fission represents the primary pathway.<sup>[2a,b,n-p]</sup> Wight et al. studied the thermal decomposition of solid RDX employing a pulsed carbon dioxide infrared (IR) laser and confirmed that the N–NO<sub>2</sub> bond dissociation represents the initial decomposition step.<sup>[2j,k]</sup> However, infrared multiphoton dissociation (IRMPD) of RDX in a molecular beam studied by Lee et al. suggested that the concerted triple C–N scission of RDX leading to three methylene nitramine (H<sub>2</sub>CNNO<sub>2</sub>) molecules represents the dominant pathway.<sup>[2c]</sup> Follow up studies exploiting a pyrolysis of solid RDX at temperatures above and below the melting point (478 K) reveal yet another decomposition pathway: the formation of a nitroso intermediate (1-nitroso-3,5-dinitrohexahydro-s-triazine; ONDNTA) that subsequently decomposes to dinitrogen oxide (N<sub>2</sub>O) and formaldehyde (H<sub>2</sub>CO).<sup>[2e]</sup> On the other hand, thermal decomposition studies by Farber et al. in a high vacuum favor the ring fragmentation pathway to methylene nitramine.<sup>[2y]</sup>

The perceptible controversies of the initial decomposition step and the products can be reconciled by suggesting that RDX

[a] Dr. S. K. Singh, J. La Jeunesse, Prof. Dr. R. I. Kaiser  
Department of Chemistry  
W. M. Keck Research Laboratory in Astrochemistry  
University of Hawaii, Honolulu, HI 96822 HI, USA  
E-mail: ralfk@hawaii.edu

[b] V. Vuppuluri, Prof. S. F. Son  
Mechanical Engineering  
Purdue Energetics Research Center, Purdue University  
West Lafayette, IN 47907, USA

[c] Dr. B.-J. Sun, Mr. Y.-L. Chen, Prof. A. H. H. Chang  
Department of Chemistry  
National Dong Hwa University  
Shoufeng, Hualien 974, Taiwan

[d] Prof. A. M. Mebel  
Department of Chemistry and Biochemistry  
Florida International University  
Miami, Florida 33199, USA

Supporting information for this article is available on the WWW under <https://doi.org/10.1002/cphc.201901202>

decomposes through multiple competing channels with one favored over the other at distinct experimental conditions (temperature, pressure, decomposition methods). The primary decomposition channels are i) elimination of dinitrogen oxide ( $\text{N}_2\text{O}$ ) and formaldehyde ( $\text{H}_2\text{CO}$ ), ii) formation of nitrogen dioxide ( $\text{NO}_2$ ), nitrogen monoxide ( $\text{NO}$ ) and higher order molecular weight products via  $\text{N}-\text{NO}_2$  fission, iii) a concerted elimination of nitrous acid ( $\text{HONO}$ ), and iv) ring fragmentation via  $\text{C}-\text{N}$  scission.<sup>[2e,q,3,6,2j,k]</sup> Therefore, from the experimental point of view, a challenging task is to avoid the presence of multiple channels by selectively opening a single decomposition pathway through tuning the experimental conditions. This approach will gain a better understanding of the initial decomposition pathway under well-defined experimental conditions as presented here.

A hitherto overlooked reason of the aforementioned discrepancies of the experimental results might be more subtle. The decomposition products of RDX were principally probed and ultimately assigned through the identification of their molecular masses after electron impact ionization of the neutral reaction products. In principle, for a given molecular mass, multiple structural isomers do exist, and traditional mass spectrometry coupled with electron impact ionization cannot always discriminate the structural isomer(s) formed.<sup>[4]</sup> These complications might be partially overcome by exploiting isotopically labeled reactants. Beheren et al. studied the thermal decomposition of isotopically labeled RDX ( $\text{RDX}-d_6$ ,  $\text{RDX}-^{13}\text{C}$ ,  $\text{RDX}-^{15}\text{N}_6$ ) to trace the products based on the mass shifts.<sup>[2f]</sup> However, postulated products observed at, for instance,  $m/z = 42$  were not confirmed by studying decomposition of  $\text{RDX}-^{18}\text{O}$ . Therefore, an alternative experimental approach to identify the nature of the structural isomers formed is required. Soft photoionization (PI) represents an ideal tool to differentiate structural isomers selectively based on their distinct adiabatic ionization energies (IE).<sup>[5]</sup> This technique has been exploited successfully to determine the structural isomers of the decomposition products of nitromethane – a model compound of nitramine-based energetic materials,<sup>[6]</sup> but, has not been utilized

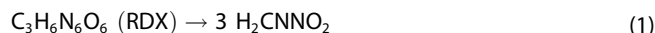
to date to elucidate the initial bond rupture processes and actual products isomer selectively in 'real' energetic materials such as for RDX under well-defined experimental conditions.

In this Communication, we exploit for the first time soft photoionization (PI) to elucidate the underlying reaction mechanism(s) and to assign the reaction products isomer selectively in the infrared multiphoton dissociation (IRMPD) of thin films of RDX in the condensed phase at 5 K. These processes are induced by a pulsed carbon dioxide ( $\text{CO}_2$ ) IR laser ( $10.6 \mu\text{m}$ ,  $6.0 \pm 0.6 \text{ mJ cm}^{-2}$  per pulse) in an ultrahigh vacuum (UHV) surface science machine operating at base pressures of  $2 \times 10^{-10}$  torr (Figure S1).<sup>[5a,7]</sup> These conditions allow the decomposition of RDX under *mild* energetic conditions opening up limited reaction channels. After the radiation exposure, infrared spectroscopy was exploited to monitor the changes in the RDX film (Figure S2, Table S1). The exposed samples were then annealed at a rate of  $1 \text{ K min}^{-1}$  to 320 K (temperature programmed desorption; TPD), and the subliming neutral products were ionized using tunable vacuum ultraviolet (VUV) photoionization (PI). The ions were separated in a reflectron time-of-flight mass spectrometer (PI-ReTOF-MS) and identified based on their mass-to-charge ratio ( $m/z$ ) by a microchannel plate detector (MCP). Fascinatingly, exploiting a photon energy of 10.49 eV, only a single mass-to-charge ratio was observed at  $m/z = 42$ . This ion was detected in previous decomposition studies of RDX utilizing electron impact ionization of the neutral decomposition products (Table 1)<sup>[2c,e,l,m,y-ab]</sup> and was assigned based on chemical intuition as diazomethane ( $\text{H}_2\text{CNN}$ )<sup>[2c,l,m,ab]</sup> and/or the radical(s)  $\text{C}_2\text{H}_4\text{N}$ <sup>[2c,y,aa]</sup> or  $\text{CNO}$ .<sup>[2e,z]</sup> In the present work, based on tunable photoionization at 10.49 eV and 9.30 eV combined with electronic structure calculations, we provide compelling evidence that  $m/z = 42$  is linked solely to ketene ( $\text{H}_2\text{CCO}$ ; IE = 9.6 eV) – a molecule with the molecular mass as diazomethane ( $\text{H}_2\text{CNN}$ ; IE = 8.9 eV). The explicit identification of ketene changes our perception how we think about the thermal decomposition mechanisms of RDX involving triple dissociation to methylene nitramine ( $\text{H}_2\text{CNNO}_2$ ) [reaction (1)], consecutive

**Table 1.** Previous assignments of signal observed at mass-to-charge ( $m/z$ ) of 42.

References	Method of decomposition	Method of ionization	Method of detection	Assignment
X. Zhao et al. <sup>[2c]</sup>	IR multiphoton dissociation using $\text{CO}_2$ laser in molecular beam ( $10.6 \mu\text{m}$ , $6-20 \text{ J cm}^{-2}$ per pulse)	Electron impact ionization	Time-of-flight mass spectrometer	$\text{CH}_2\text{N}_2/\text{C}_2\text{H}_4\text{N}$
J. T. Dickinson et al. <sup>[2l]</sup>	KrF excimer laser radiation of RDX crystals ( $248 \text{ nm}$ , $< 5 \text{ mJ cm}^{-2}$ )	Electron impact ionization	Quadrupole mass spectrometer	$\text{CH}_2\text{N}_2/\text{C}_2\text{H}_4\text{N}$
R. Behrens et al. <sup>[2f]</sup>	Thermal decomposition at 465 K	Electron impact ionization	Quadrupole mass spectrometer	CNO
T. B. Tang et al. <sup>[2m]</sup>	Photolysis at 266 nm laser ( $\sim 500 \mu\text{J}$ )	Multiphoton ionization	Time-of-flight mass spectrometer	$\text{CH}_2\text{N}_2$
M. Farber et al. <sup>[2y]</sup>	Thermal decomposition at 473 K	Electron impact ionization	Quadrupole mass spectrometer	$\text{C}_2\text{H}_4\text{N}$
L. Zhou et al. <sup>[2z]</sup>	Rapid heating with a heating rate of $\sim 10^5 \text{ K s}^{-1}$	Electron impact ionization	Time-of-flight mass spectrometer	$\text{C}_2\text{H}_4\text{N}$ , $\text{CH}_2\text{N}_2$ , CNO
P. A. Snyder et al. <sup>[2aa]</sup>	Pyrolysis at 633 K	Atmospheric pressure chemical ionization	Quadrupole mass spectrometer	$\text{C}_2\text{H}_4\text{N}$
H. Ostmark et al. <sup>[2ab]</sup>	$\text{CO}_2$ Laser pyrolysis ( $10.6 \mu\text{m}$ , 180 W)	Electron impact ionization	Quadrupole mass spectrometer	$\text{CH}_2\text{N}_2/\text{C}_2\text{H}_4\text{N}$
W. Zhang et al. <sup>[19]</sup>	Laser irradiation (1064 nm, 800 mJ)	Multiphoton ionization	Time-of-flight mass spectrometer	$\text{C}_2\text{H}_4\text{N}/\text{CNO}$

decomposition to formaldehyde ( $\text{H}_2\text{CO}$ ) and dinitrogen monoxide ( $\text{N}_2\text{O}$ ) [reaction (2)], and reaction of two formaldehyde molecules leading to ketene ( $\text{H}_2\text{CCO}$ ) plus water ( $\text{H}_2\text{O}$ ) [reaction (3)]. This key result highlights the necessity to elucidate the identity of the true decomposition products exploiting tunable vacuum ultraviolet photoionization.



Infrared spectroscopy was employed to analyze the  $15.5 \pm 1.0 \mu\text{m}$  thick RDX samples before and after the exposure to the carbon dioxide laser (Experimental Methods). The infrared spectrum of RDX recorded at 5 K prior to the irradiation reveals prominent vibrational bands in the region  $4000\text{--}600 \text{ cm}^{-1}$  (Figure S2; Table S1) characteristic of amorphous RDX as evident from the band broadening. The crystalline phases of RDX exhibit sharp infrared absorptions (Figure S3). In the amorphous sample, absorption features at  $3079$  and  $2994 \text{ cm}^{-1}$  correspond to  $\text{CH}_2$  asymmetric and symmetric stretching modes respectively. A broad absorption band observed from  $1590$  to  $1531 \text{ cm}^{-1}$  can be attributed to the asymmetric vibrations of nitro group ( $-\text{NO}_2$ ). The  $\text{N}-\text{NO}_2$  stretching vibration of RDX appears at  $1319 \text{ cm}^{-1}$ , while ring vibrations dominate the spectral regions of  $1217\text{--}1173 \text{ cm}^{-1}$ ,  $1080\text{--}908 \text{ cm}^{-1}$  and  $848\text{--}667 \text{ cm}^{-1}$ . The infrared spectrum measured after the irradiation at high dose display only a small minor ( $8 \pm 1\%$ ) decrease in the intensity of the RDX vibrational bands (Figure S2). In addition, a new broad absorption feature appears in the region  $3513\text{--}3203 \text{ cm}^{-1}$ , which is linked to  $\text{O}-\text{H}$  stretching vibration of water ( $\text{H}_2\text{O}$ ). Considering the small decomposition fraction of RDX and the sole detection of the strong infrared absorber water ( $\text{H}_2\text{O}$ ), prominent absorptions of less infrared sensitive products might be masked by the absorption of the RDX reactant. Therefore, to detect additional degradation products, a highly sensitive analytical technique such as soft photoionization (PI) coupled with reflectron time-of-flight mass spectrometry (PI-ReTOF-MS) is applied.

The temperature-dependent mass spectra of the decomposition products subliming from the irradiated RDX samples are depicted in Figure 1. The mass spectra were collected at a photoionization energy of  $10.49 \text{ eV}$  and revealed sole signal at  $m/z=42$ . The corresponding TPD profiles for the high dose and low dose experiments are depicted in Figures 2a and 2b respectively. The control experiment, i.e. an experiment performed under identical conditions but without exposing the RDX samples to the infrared laser, does not reveal any ion counts at all at  $m/z=42$  (Figure S4). This finding suggests that signal observed at  $m/z=42$  is the result of the exposure of RDX to the infrared laser. Ion counts at  $m/z=42$  can be ascribed to two molecules: diazomethane ( $\text{H}_2\text{CNN}$ ) and ketene ( $\text{H}_2\text{CCO}$ ). To identify which isomer(s) is(are) actually formed in the experiment, we selectively photoionize the isomer(s) based on their ionization energies. The adiabatic ionization energies of ketene ( $\text{H}_2\text{CCO}$ ;  $\text{IE}=9.6 \text{ eV}$ ) and diazomethane ( $\text{H}_2\text{CNN}$ ;  $\text{IE}=8.9 \text{ eV}$ ) are separated

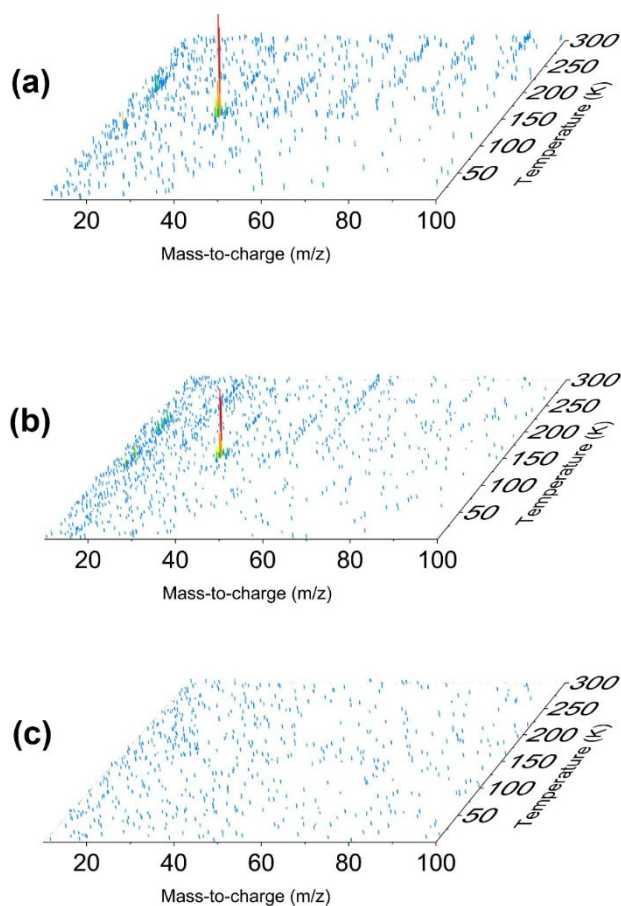


**Figure 1.** PI-ReTOF-MS data recorded at high dose (a) and low dose (b, c) experiments at photoionization energies of  $10.49 \text{ eV}$  (a, b) and  $9.30 \text{ eV}$  (c).

by  $0.7 \text{ eV}$ . At a photoionization energy of  $10.49 \text{ eV}$  both the isomers can be ionized. However, a photoionization energy of  $9.30 \text{ eV}$  permits only the ionization of diazomethane ( $\text{H}_2\text{CNN}$ ). The mass spectra collected at a photoionization energy of  $9.30 \text{ eV}$  after the irradiation of RDX sample do not reveal any ion counts at  $m/z=42$  (Figures 1c and 2c). Therefore, we can conclude that diazomethane ( $\text{H}_2\text{CNN}$ ) is not observed, and the ion signal at  $m/z=42$  is solely linked to ketene ( $\text{H}_2\text{CCO}$ ).

Considering the molecular structure of RDX (Scheme 1) and of the detected reaction products ( $\text{H}_2\text{O}$ ,  $\text{H}_2\text{CCO}$ ), it is intriguing to unravel the underlying reaction mechanism(s) through ab initio calculations at the B3LYP/cc-pVTZ//CCSD(T)/CBS level of theory (Figures 3 and 4; Computational Methods in the Supporting Information). The experimental results can be reconciled by an initially decomposition of the RDX molecule through ring fragmentation via a triple concerted C–N bond scission to form three molecules of methylene nitramine ( $\text{H}_2\text{CNNO}_2$ ). The electronic structure calculations suggest that the concerted ring fragmentation pathway connects via a transition state located  $264 \text{ kJ mol}^{-1}$  above the separated products formed in an overall endoergic reaction ( $+194 \text{ kJ mol}^{-1}$ ) (Figure S5). These energetics are in close agreement with those of Goddard et al. computed at the B3LYP/6-

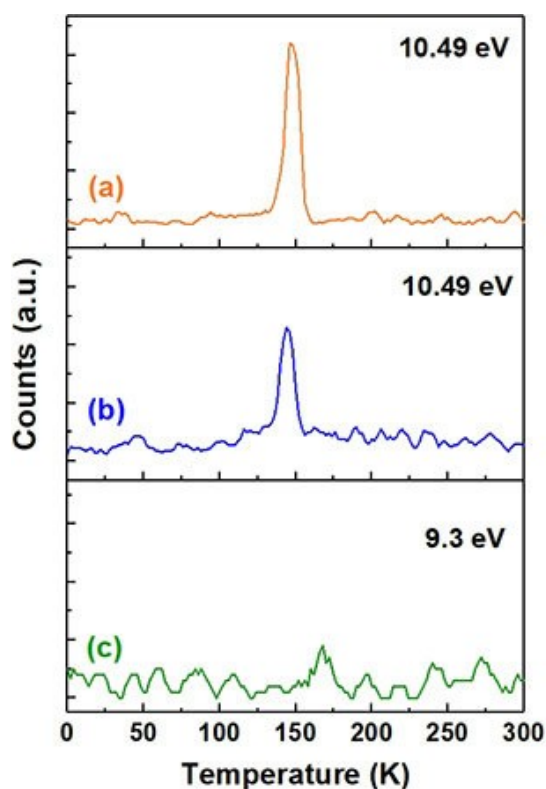


**Figure 2.** TPD profiles recorded at mass-to-charge ratio of 42 in a) high dose and b) low dose experiments at a photoionization energy of 10.49 eV. c) TPD profile recorded in the high dose study at a photoionization energy of 9.30 eV.

31G(d) level of theory.<sup>21</sup> Our calculations predict that methylene nitramine ( $\text{H}_2\text{CNNO}_2$ ) can further undergo infrared-assisted decomposition (Figure 3). This pathway involves an atomic oxygen shift from the  $-\text{NO}_2$  moiety to the methylene group ( $\text{CH}_2$ ) resulting in an exotic cyclic intermediate **I1** ( $c\text{-OCH}_2\text{NNO}$ ) through a barrier of  $123 \text{ kJ mol}^{-1}$  in an endoergic reaction ( $+32 \text{ kJ mol}^{-1}$ ). This intermediate already holds key functional groups and decomposes easily through a transition state located  $81 \text{ kJ mol}^{-1}$  above  $c\text{-OCH}_2\text{NNO}$  to dinitrogen oxide ( $\text{N}_2\text{O}$ ) and formaldehyde ( $\text{H}_2\text{CO}$ ). The structure of exotic intermediate **I1** needs some attention here. It has a distorted four membered ring structure where the N–O bond of the ring is elongated holding a bond length of  $145 \text{ pm}$ ; this indicates a strong single bond character; the N–N bond length in the ring is  $128 \text{ pm}$  thus representing a partial double bond character. The C–O and C–N bond lengths in the ring are very similar ( $146 \text{ pm}$ ). Selected molecular orbitals of intermediate **I1** are provided in Figure S9 of the Supporting Information, which depicts electron density over the ring and heteroatoms. Note that although the decomposition of methylene nitramine ( $\text{H}_2\text{CNNO}_2$ ) is overall exoergic ( $-165 \text{ kJ mol}^{-1}$ ), formation of **I1** requires a barrier of  $123 \text{ kJ mol}^{-1}$ . Considering that a barrier of  $264 \text{ kJ mol}^{-1}$  has to be overcome in the aforementioned concerted triple dissociation of RDX, the transition state linking methylene nitramine ( $\text{H}_2\text{CNNO}_2$ ) and intermediate **I1** through a barrier of only

$123 \text{ kJ mol}^{-1}$  can be easily overcome under our experimental conditions.

This finding implies that this dissociation pathway is highly favorable compared to the decomposition leading to the non-detected diazomethane ( $\text{H}_2\text{CNN}$ ) and singlet oxygen ( $\text{O}_2$ ;  $a^1\Delta_g$ ) channel. The latter would require passing multiply high-energy transition states ranging up to  $394 \text{ kJ mol}^{-1}$  above the methylene nitramine reactant. In detail, methylene nitramine may undergo unimolecular decomposition via a cyclic intermediate **I2** ( $c\text{-H}_2\text{CNNO}_2$ ) and an acyclic isomer **I3** ( $\text{H}_2\text{CNNOO}$ ) yielding of diazomethane and oxygen (Figure 3). To access intermediate **I2** an energy of  $394 \text{ kJ mol}^{-1}$  is required. Intermediate **I2** may dissociate in one step to diazomethane ( $\text{H}_2\text{CNN}$ ) and oxygen ( $\text{O}_2$ ) after overcoming an energy barrier of  $391 \text{ kJ mol}^{-1}$ ; alternatively, intermediate **I2** may ring-open to **I3**, which requires a barrier of  $81 \text{ kJ mol}^{-1}$  to overcome. Then, intermediate **I3** can decompose to  $\text{H}_2\text{CNN}$  (diazomethane) plus  $\text{O}_2$  (oxygen) in an overall exoergic reaction of  $257 \text{ kJ mol}^{-1}$  with respect to the reactant. Therefore, these considerations reveal that the unimolecular decomposition of methylene nitramine ( $\text{H}_2\text{CNNO}_2$ ) into diazomethane ( $\text{H}_2\text{CNN}$ ) and oxygen ( $\text{O}_2$ ) is much less favorable compared to the decomposition into dinitrogen monoxide ( $\text{N}_2\text{O}$ ) and formaldehyde ( $\text{H}_2\text{CO}$ ).

What is the ultimate fate of formaldehyde ( $\text{H}_2\text{CO}$ )? Two formaldehyde ( $\text{H}_2\text{CO}$ ) molecules may react to form eventually ketene ( $\text{H}_2\text{CCO}$ ) and water ( $\text{H}_2\text{O}$ ); the energetically most favorable section of the potential energy surfaces is revealed in Figure 4. In principal, two molecules of formaldehyde ( $\text{H}_2\text{CO}$ ) can react to form methanol ( $\text{CH}_3\text{OH}$ ) and carbon monoxide ( $\text{CO}$ ) via a transition state located  $99 \text{ kJ mol}^{-1}$  above the reactants. Carbon monoxide and methanol can react further to ketene ( $\text{H}_2\text{CCO}$ ) and water ( $\text{H}_2\text{O}$ ) in a concerted reaction; this requires a transition state of  $246 \text{ kJ mol}^{-1}$  to be overcome. Alternatively, two molecules of formaldehyde may react to form 2-hydroxyacetaldehyde ( $(\text{OH})\text{H}_2\text{CCHO}$ ), which can dissociate into water ( $\text{H}_2\text{O}$ ) and ketene ( $\text{H}_2\text{CCO}$ ). However, this reaction requires an energy of at least  $317 \text{ kJ mol}^{-1}$  to overcome the transition state. Once again, considering that  $264 \text{ kJ mol}^{-1}$  have to be incorporated to pass the inherent barrier for the concerted triple dissociation of RDX, the highest barrier in the reaction of two formaldehyde molecules to water and ketene only ranges at  $174 \text{ kJ mol}^{-1}$ . Therefore, formation of ketene from two formaldehyde molecules via methanol ( $\text{CH}_3\text{OH}$ ) and carbon monoxide ( $\text{CO}$ ) is energetically more viable than the mechanism involving 2-hydroxyacetaldehyde ( $(\text{OH})\text{H}_2\text{CCHO}$ ). It is important to recall that previous studies reported dinitrogen oxide ( $\text{N}_2\text{O}$ ) and formaldehyde ( $\text{H}_2\text{CO}$ ) at dominating decomposition products at relatively low temperatures less than  $450 \text{ K}$ .<sup>[8]</sup> The  $200 \mu\text{s}$  pulse width carbon dioxide laser operating at low laser fluence of  $6.0 \pm 0.6 \text{ mJ cm}^{-2}$  employed in the present study suggests a low heating rate (Table S2).

In conclusion, the infrared multiphoton dissociation of RDX to eventually ketene ( $\text{H}_2\text{CCO}$ ) and water ( $\text{H}_2\text{O}$ ) accompanied with dinitrogen monoxide ( $\text{N}_2\text{O}$ ) opens up a hitherto elusive decomposition pathway under experimentally *mild* fragmentation conditions. The proposed decomposition is initiated by the triple dissociation of RDX to three molecules of methylene

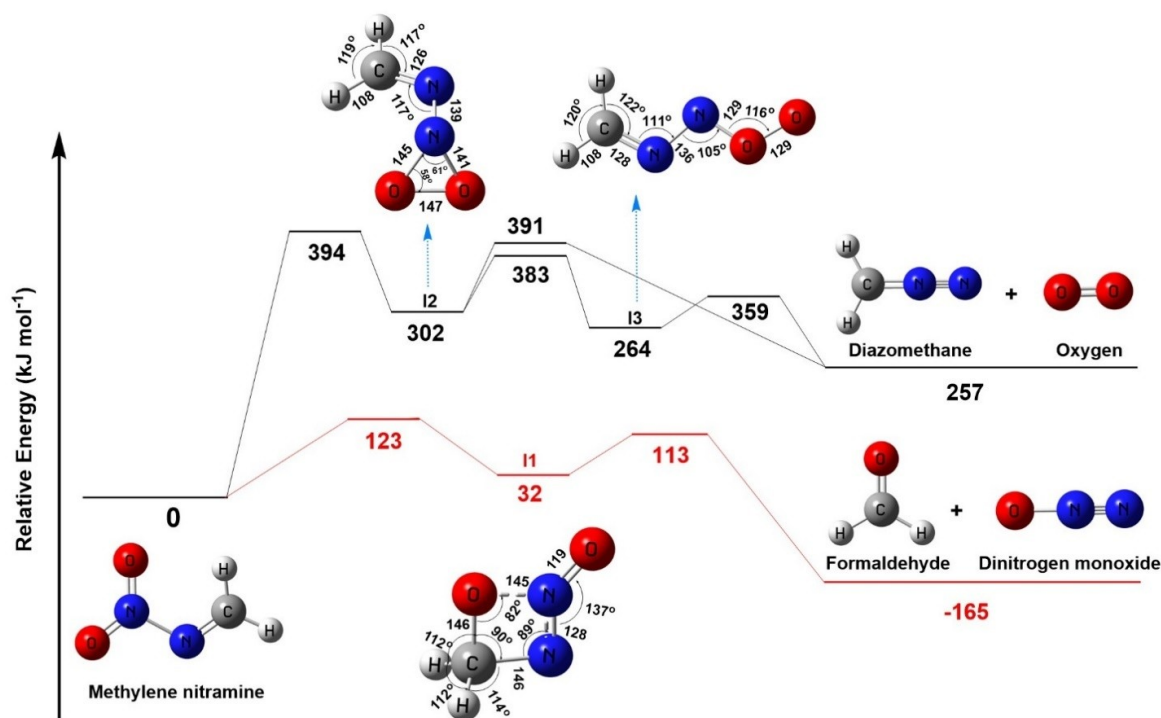


**Figure 3.** Computed decomposition mechanism of methylene nitramine ( $\text{H}_2\text{CNNO}_2$ ). The pathway leading to diazomethane ( $\text{H}_2\text{CNN}$ ) and singlet oxygen ( $\text{O}_2$ ;  $a^1\Delta_g$ ) is shown in black while the route to formaldehyde ( $\text{H}_2\text{CO}$ ) and dinitrogen monoxide ( $\text{N}_2\text{O}$ ) is represented in red. Bond lengths are in pm and bond angles are in degree. Geometrical parameters of reactant and products are provided in Figure S7 of the Supporting Information.

nitramine ( $\text{H}_2\text{CNNO}_2$ ), which subsequently undergoes decomposition to formaldehyde ( $\text{H}_2\text{CO}$ ) and dinitrogen monoxide ( $\text{N}_2\text{O}$ ) via an exotic acyclic reaction intermediate **I1**. Two formaldehyde molecules then eventually undergo multi photon induced reaction to ketene ( $\text{H}_2\text{CCO}$ ) and water ( $\text{H}_2\text{O}$ ). The ultimate evidence on the formation of water and ketene during RDX decomposition was obtained by exploiting infrared spectroscopy (water) and isomer selective single photoionization reflectron time-of-flight mass spectrometry (ketene). Based on tunable photoionization at 10.49 eV and 9.30 eV, the experiments revealed signal at  $m/z = 42$  – previously incorrectly associated to diazomethane ( $\text{H}_2\text{CNN}$ ) – solely linked to ketene ( $\text{H}_2\text{CCO}$ ) thus highlighting the necessity to exploit isomer-selective detection tools to probe the decomposition of RDX via overall equations (1)–(3) (Figures 3 and 4). Operating under the premise that reaction intermediate **I1** is unstable and methanol, carbon monoxide, and formaldehyde convert to ketene plus water, at least dinitrogen monoxide ( $\text{N}_2\text{O}$ ) should represent a co-product. Considering its ionization energy of 12.89 eV, dinitrogen monoxide cannot be photo ionized at 10.49 eV; also, it was not observable infrared spectroscopically. Considering the infrared modes and integrated absorption coefficients of dinitrogen monoxide and the experimentally detected water production, signal calculations reveal that dinitrogen monoxide abundances are below the detection limit of the infrared setup (Figure S2, Quantitative Analysis). Considering that the elementary mechanisms involved in the decomposition of RDX are very complex, our approach technique could be useful in prospec-

tive studies determining the structure and hence nature of the isomer(s) of primary and higher order decomposition products of RDX eventually aid in resolving the prevailing discrepancies associated with the decomposition pathway of nitramine-based energetic materials.

## Conflict of Interest

There are no conflicts to declare.

## Acknowledgments

This project was supported by the U.S. Army Research Office (ARO) (W911NF1810438). B.J.S. and A.H.H.C. appreciate the National Center for High-performance Computer in Taiwan for providing the computer resources in the calculations.

## Conflict of Interest

The authors declare no conflict of interest.

**Keywords:** ab initio calculations · infrared multiphoton dissociation · mass-spectrometry · photoionization · RDX

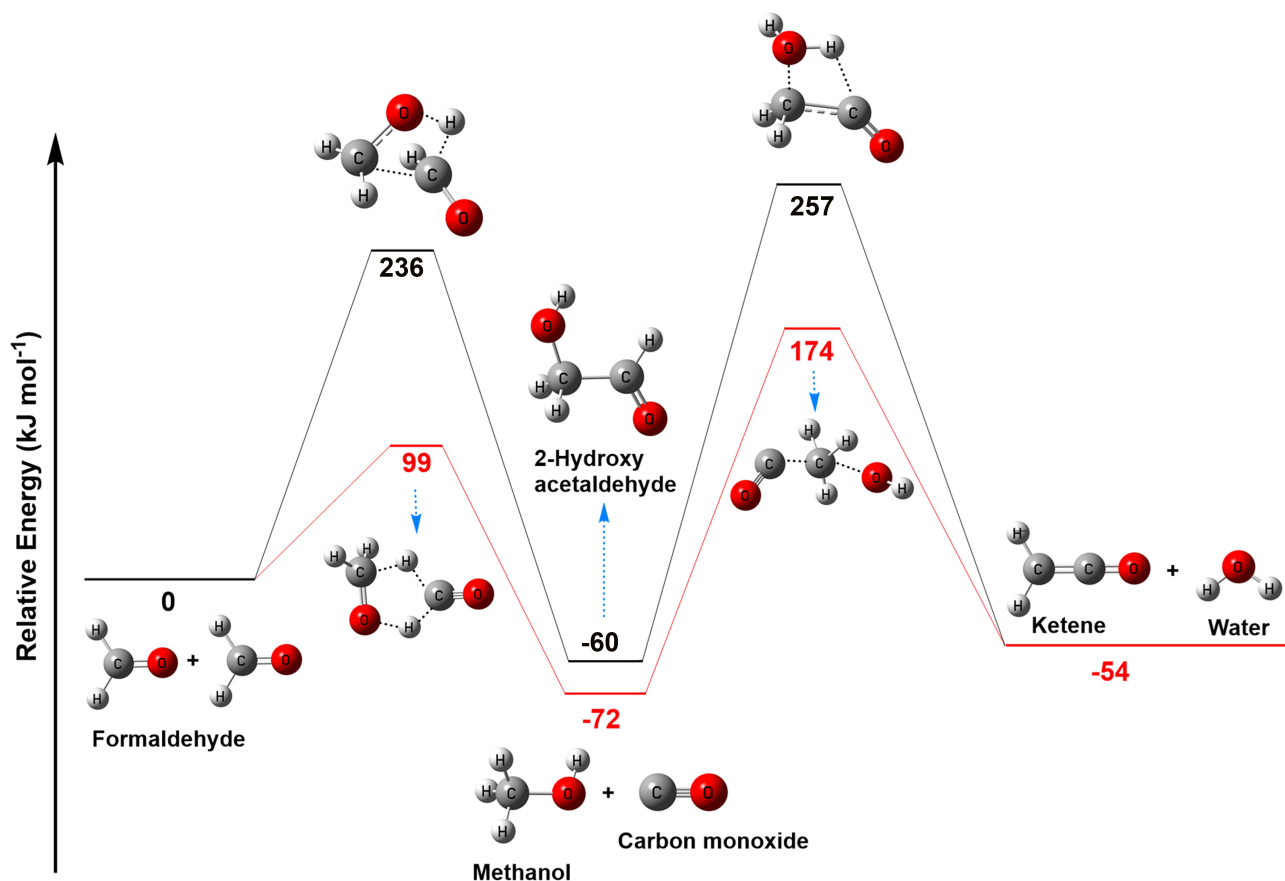


**Figure 4.** Computed formation pathways of ketene ( $\text{H}_2\text{CCO}$ ) and water ( $\text{H}_2\text{O}$ ) from formaldehyde. Geometrical parameters of reactants, products and intermediates are provided in Figure S8 of the Supporting Information.

- [1] a) G. F. Adams, R. W. Shaw, *Annu. Rev. Phys. Chem.* **1992**, *43*, 311–340; b) (Ed.: D. S. George Olah), Academic Press, San Diego, **1991**; c) (Ed.: S. N. Bulusu), Springer Netherlands, **1990**.
- [2] a) M. Greenfield, Y. Q. Guo, E. R. Bernstein, *Chem. Phys. Lett.* **2006**, *430*, 277–281; b) Y. Q. Guo, M. Greenfield, A. Bhattacharya, E. R. Bernstein, *J. Chem. Phys.* **2007**, *127*, 154301; c) X. Zhao, E. J. Hints, Y. T. Lee, *J. Chem. Phys.* **1988**, *88*, 801–810; d) G. W. Lemire, J. B. Simeonsson, R. C. Sausa, *Anal. Chem.* **1993**, *65*, 529–533; e) R. Behrens, S. Bulusu, *J. Phys. Chem.* **1992**, *96*, 8877–8891; f) R. Behrens, S. Bulusu, *J. Phys. Chem.* **1992**, *96*, 8891–8897; g) S. Maharrey, R. Behrens, *J. Phys. Chem. A* **2005**, *109*, 11236–11249; h) H. Zuckermann, G. D. Greenblatt, Y. Haas, *J. Phys. Chem.* **1987**, *91*, 5159–5161; i) M. Miao, Z. A. Dreger, J. E. Patterson, Y. M. Gupta, *J. Phys. Chem. A* **2008**, *112*, 7383–7390; j) T. R. Botcher, C. A. Wight, *J. Phys. Chem.* **1993**, *97*, 9149–9153; k) Y. Lee, C.-J. Tang, T. A. Litzinger, *Combust. Flame* **1999**, *117*, 600–628; l) J. T. Dickinson, L. C. Jensen, D. L. Doering, R. Yee, *J. Appl. Phys.* **1990**, *67*, 3641–3651; m) T. B. Tang, M. M. Chaudhri, C. S. Rees, S. J. Mullock, *J. Mater. Sci.* **1987**, *22*, 1037–1044; n) N. C. Dang, J. L. Gottfried, F. C. De Lucia, *Appl. Opt.* **2017**, *56*, B85–B91; o) C. Capellos, P. Papagiannakopoulos, Y.-L. Liang, *Chem. Phys. Lett.* **1989**, *164*, 533–538; p) K. L. Gares, S. V. Bykov, T. Brinzer, S. A. Asher, *Appl. Spectrosc.* **2015**, *69*, 545–554; q) D. Chakraborty, R. P. Muller, S. Dasgupta, W. A. Goddard, *J. Phys. Chem. A* **2000**, *104*, 2261–2272; r) M. J. Swadley, T. Li, *J. Chem. Theory Comput.* **2007**, *3*, 505–513; s) I. V. Schweigert, *J. Phys. Chem. A* **2015**, *119*, 2747–2759; t) O. Sharia, M. M. Kuklja, *J. Phys. Chem. A* **2010**, *114*, 12656–12661; u) N. J. Harris, K. Lammertsma, *J. Am. Chem. Soc.* **1997**, *119*, 6583–6589; v) A. Bhattacharya, E. R. Bernstein, *J. Phys. Chem. A* **2011**, *115*, 4135–4147; w) K. K. Irikura, *J. Phys. Chem. A* **2013**, *117*, 2233–2241; x) B. M. Rice, G. F. Adams, M. Page, D. L. Thompson, *J. Phys. Chem.* **1995**, *99*, 5016–5028; y) M. Farber, R. D. Srivastava, *Chem. Phys. Lett.* **1979**, *64*, 307–310; z) L. Zhou, N. Piekielek, S. Chowdhury, M. R. Zachariah, *Rapid Commun. Mass Spectrom.* **2009**, *23*, 194–202; aa) A. P. Snyder, J. H. Kremer, S. A. Liebman, M. A. Schroeder, R. A. Fifer, *Org. Mass Spectrom.* **1989**, *24*, 15–21; ab) H. Östmark, H. Bergman, K. Ekvall, *J. Anal. Appl. Pyrolysis* **1992**, *24*, 163–178; ac) S. K. Singh, C. Zhu, V. Vuppuluri, S. F. Son, R. I. Kaiser, *J. Phys. Chem. A* **2019**, *123*, 9479–9497.
- [3] R. W. Molt, T. Watson, A. P. Bazanté, R. J. Bartlett, N. G. J. Richards, *Phys. Chem. Chem. Phys.* **2016**, *18*, 26069–26077.
- [4] a) M. J. Abplanalp, M. Förstel, R. I. Kaiser, *Chem. Phys. Lett.* **2016**, *644*, 79–98; b) O. Kostko, B. Bandyopadhyay, M. Ahmed, *Annu. Rev. Phys. Chem.* **2016**, *67*, 19–40.
- [5] a) B. M. Jones, R. I. Kaiser, *J. Phys. Chem. Lett.* **2013**, *4*, 1965–1971; b) R. I. Kaiser, S. Maity, B. M. Jones, *Phys. Chem. Chem. Phys.* **2014**, *16*, 3399–3424.
- [6] a) P. Maksyutenko, L. G. Muzangwa, B. M. Jones, R. I. Kaiser, *Phys. Chem. Chem. Phys.* **2015**, *17*, 7514–7527; b) P. Maksyutenko, M. Förstel, P. Crandall, B.-J. Sun, M.-H. Wu, A. H. H. Chang, R. I. Kaiser, *Chem. Phys. Lett.* **2016**, *658*, 20–29; c) R. I. Kaiser, P. Maksyutenko, *Chem. Phys. Lett.* **2015**, *631–632*, 59–65; d) R. I. Kaiser, P. Maksyutenko, *J. Phys. Chem. C* **2015**, *119*, 14653–14668.
- [7] a) C. J. Bennett, S. J. Brotton, B. M. Jones, A. K. Misra, S. K. Sharma, R. I. Kaiser, *Anal. Chem.* **2013**, *85*, 5659–5665; b) A. Bergantini, M. J. Abplanalp, P. Pokhilko, A. I. Krylov, C. N. Shingledecker, E. Herbst, R. I. Kaiser, *Astrophys. J.* **2018**, *860*, 108.
- [8] T. B. Brill, *J. Propul. Power* **1995**, *11*, 740–751.
- [9] W. Zhang, R. Shen, Y. Ye, L. Wu, Y. Hu, P. Zhu, *Spectrosc. Lett.* **2014**, *47*, 611–615.

Manuscript received: December 19, 2019  
 Revised manuscript received: February 18, 2020  
 Version of record online: March 29, 2020